# MAGNETOMETRY USING ELECTROMAGNETICALLY INDUCED TRANSPARENCY IN A ROOM TEMPERATURE VAPOUR CELL

## Developing an Optical Magnetometer that Utilises the Steep Dispersion Curve Observed in EIT to Detect Time Varying Magnetic Fields

Melody R. Blackman and Benjamin T. H. Varcoe

*School of Physics and Astronomy, University of Leeds, Leeds LS2 9JT, U.K.*

Keywords: Magnetometry, EIT.

Abstract: The physiological importance of magnetic signals within biological systems has been investigated with ever increasing sensitivities over the last decade. Currently superconducting quantum interference devices (SQUIDs) are at the forefront of bio-magnetic diagnostics. In this research we aim to build an optics based magnetometer that can compete with the sensitivity of the SQUID but that runs at a lower start up and operational cost. To do this we intend to use the steep dispersion curve observed in the atomic physics effect electromagnetically induced transparency. This magnetometer can operate at room temperature, its design is a convenient method for monitoring bio-magnetic fields, making this technology an affordable technique for further bio-magnetic diagnostics.

## 1 INTRODUCTION

Bio-magnetism is a fast developing field of research as its non-invasive applications make it a very desirable diagnostic tool. The presence of time varying electric fields in the human body has been greatly studied over the last hundred years. Electrocardiographs (ECG) measure these fields as potential differences on the skin's surface, with emphasis on the torso (Nash et al., 2002; Ramanathan et al., 2004). However each of these electric fields is accompanied by a weak magnetic field that also holds information on the condition of the organ. Unlike electric fields the magnetic, do not suffer from varying attenuation at they travel through the different types of tissue. Another advantage of measuring the magnetic field is the ability to make direct measurements of an organ's field map instead of the potential difference between two points.

The largest magneto-physiological signal in the body is created by the heart's QRS peak which corresponds to the contraction and relaxation of the cardiac muscle during a single heart beat. The magnetic fields associated with this process are of the order of tens of picotesla, although the more clinically important signals that are unobservable with ECG are formed by the cardiac conducting system, which are superimposed on the field and are less than 1 pT (Fenici et al., 1983).

Currently at the forefront of magnetometer clinical trials are Superconducting Quantum Interference Devices (SQUIDs), which have displayed sensitivities as high a few fT/$\sqrt{Hz}$ (Vodel and Makiniemi, 1992). Since their implementation they have been used to form dynamic mapping of both the brain and heart's magnetic fields (Hämäläinen et al., 1993; Fagaly, 2006). The limitations with SQUIDs come from their operational requirements, starting with their need for a cryostat, crucial for the 4 Kelvin cooling of the superconducting materials that make up the Josephson junctions used in the detector heads. This causes the overall cost of the SQUIDs to be very high (in the order of hundreds of thousands of pounds) meaning there is a place in the market for cheaper alternatives.

It is in the field of optical magnetometry where the most promising competition to SQUIDs can be found (Bloom, 1962; Cohen-Tannoudji et al., 1969; Nagel et al., 1998; Budker et al., 2000; Bison et al., 2003; Kominis et al., 2003) and it is in this field that our research is based. These methods allow for low cost, non-invasive, non-contact highly sensitive magnetic field detectors that can be made and operated at a fraction of the cost of a SQUID. The ability to measure bio-magnetic signals without contact makes

it very useful for fetal cardiac diagnostics (Comani et al., 2004) as well as the more standard magneto-cardiographs (MCG) and in the case of burns victims where contact is not an option.

When making observations of magnetic fields using atom-light interactions one may start by thinking of the Zeeman effect. The Zeeman effect explains the perturbation of atomic energy levels by means of an applied magnetic field, which couples to the magnetic moment of the atomic electrons. Here we still utilise the Zeeman effect but we need to go further into the detail of the energy level shifts by discussing the ac-Stark shift (also called the Autler-Townes effect) as these are essential to the mechanism needed for making our magnetometer more sensitive than a device utilising just the Zeeman effect.

In this experiment we use a form of coherent population trapping (CPT) (Belfi et al., 2007) called Electromagnetically Induced Transparency (EIT) (Boller et al., 1991; Scully, 1991; Harris, 1997). EIT is a quantum interference effect whereby an opaque medium is made transparent to a probe laser under certain resonance conditions. To understand how the many mechanisms that create EIT work together we shall start by considering a three level system in the $\Lambda$ configuration. A depiction of the $\Lambda$ transition used in this experiment is displayed in figure 1. In this case the ground states are degenerate, resulting in a symmetric transition so the coupling and probe beams can be resonant with either $m_F = \pm 1$ levels by switching the sign of the circular polarisation ($\sigma^{+/-}$).

The intense coupling beam drives the transition into the excited state; at this point an ac Stark shift occurs at the upper energy level, whereby the atomic absorption line splits into an Autler-Townes doublet, symmetric about the transition's unshifted resonance.

We now consider the processes of EIT in more detail. We are fortunate that a thorough mathematical understanding of EIT is available allowing us to simulate the system before building an experiment. This is presented in the following paragraphs.

The following time dependent interaction Hamiltonian describes the atom-light coupling for a system with EIT;

$$H_{int} = -\frac{\hbar}{2}[\Omega_p(t)\hat{\sigma}_{eg_1}e^{i\Delta_1 t} + \Omega_c(t)\hat{\sigma}_{eg_2}e^{i\Delta_2 t} + H.c]$$
(1)

where the $\Omega_{c/p}(t)$ are the Rabi frequencies of the coupling and probe fields respectively, $\hat{\sigma}_{ij} = |i\rangle\langle j|$ is the atomic projection operator, $\Delta$ is the detuning and H.c is the Hermitian conjugate. It is this Hamiltonian that is inserted into the Master equation and allows us to calculate the atomic density operators ($\rho$). The solutions of the Master equation are fundamental
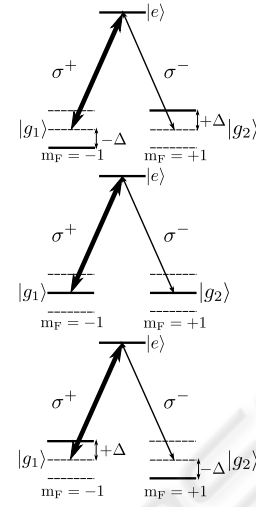


Figure 1: The $\Lambda$ configuration for our $^{87}Rb$ transition showing the possible detuning ($\Delta$) of the $m_F$ levels in the presence of a coupling and probe beam. $\sigma^{+/-}$ denotes the sign of the circular polarisation. As the applied magnetic field oscillates our system will rotate through these three $\Lambda$ systems.

to understanding how the photons are no longer absorbed at the resonance peak, showing us that when the coupling and probe beams interact they can cancel each others absorptive terms producing a dark state by means of destructive quantum interference. How this affects the absorption can be seen by looking at the real and imaginary parts of the linear susceptibility ($\chi$), given by;

$$\chi(-\omega_p, \omega_p) = \frac{|\mu_{13}|^2}{\varepsilon_0 \hbar}\frac{N_{atom}}{V}$$
$$\times \left[ \frac{4\delta(|\Omega|^2 - 4\delta\Delta) - 4\Delta\gamma_{g_1g_2}^2}{||\Omega|^2 + (\gamma_{eg_1} + i2\Delta)(\gamma_{g_1g_2} + i2\delta)|^2} \right.$$
$$\left. +i\frac{8\delta^2\gamma_{eg_1} + 2\gamma_{g_1g_2}(|\Omega|^2 + \gamma_{g_1g_2}\gamma_{eg_1})}{||\Omega|^2 + (\gamma_{eg_1} + i2\Delta)(\gamma_{g_1g_2} + i2\delta)|^2} \right]$$
(2)

where the two photon detuning, $\delta = \Delta_1 - \Delta_2 = \omega_{g_1g_2} - (\omega_p - \omega - c)$ and is derived from the single photon detuning, $\Delta = \Delta_1 = \omega_{eg_1} - \omega_p$. The coherent decay between states is $\gamma$, in this case $\gamma_{g_1}\gamma_{g_2} = 0$. The probe beam term ($\gamma_e\gamma_{g2}$) is neglected from the equation as it is assumed it has no observable effect on the atom's behaviour, this is in part due to the two photon Raman resonance which occurs in the presence of the dark states (Fleischhauer et al., 2005).

The linear susceptibility, as seen in equation 2 holds all the important information about the atom's absorption and refractive index and as these are both

MAGNETOMETRY USING ELECTROMAGNETICALLY INDUCED TRANSPARENCY IN A ROOM
TEMPERATURE VAPOUR CELL - Developing an Optical Magnetometer that Utilises the Steep Dispersion Curve
Observed in EIT to Detect Time Varying Magnetic Fields
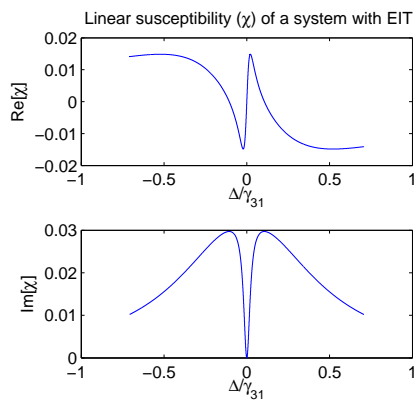
Figure 2: This figure shows first the real Re[χ] then the imaginary Im[χ] parts of the susceptibility calculated for the D1 line of $^{87}$Rb using equation 2.

altered in a EIT system it gives us a clear picture of how the atom-light interaction has changed. Figure 2 displays how all these effects alter the real (Re[χ]) and the imaginary (Im[χ]) part of χ.
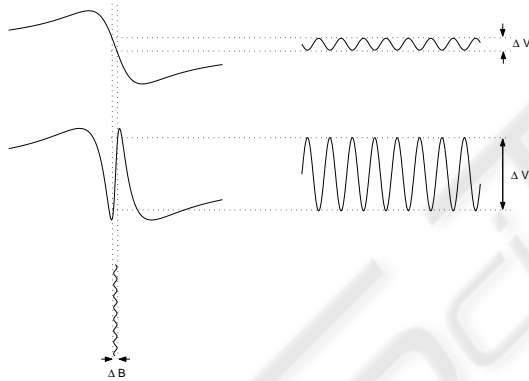


Figure 3: The top line is a representation of Re[χ] for a standard saturation spectroscopy dispersion curve, while the lower is Re[χ] in the presence of EIT. The figure displays how the sensitivity to magnetic field is increased proportionally to the gradient of the dispersion curve, where ΔB is the amplitude of the input and ΔV is the amplitude of the response.

The key to why a system with EIT makes for a good magnetometer is the steep dispersion curve. Figure 3 shows a representation of the difference that the steep dispersion curve has on the atom's response to magnetic fields. Therefore the steeper one can make the dispersion curve the better the magnetic detector will be produced from it.

## 2 EXPERIMENTAL SETUP

The experiment currently runs using free space optics and a diode laser. The laser is tuned to 794.985nm, which is the transition frequency of the D1 ($5^2S_{1/2(F=2)}5^2P_{1/2(F=1)}$) line of rubidium 87 ($^{87}$Rb). The $^{87}$Rb is contained within vapour cell with a buffer gas of, neon at 30Torr. We use $^{87}$Rb as it allows us the run the experiment at room temperature with low powered laser beams. Figure 4 displays the apparatus used in this experiment.

The laser is a commercially available diode laser, from which beams are tapped off and sent to the diagnostic and stabilisation section of the experiment. Contained within this setup is the reference $^{85/87}$Rb vapour cell, arranged in a saturation spectroscopy retro-reflection configuration. Using this along with a wavemeter and a lock-in amplifier we can lock the laser to the resonance peak of the transition, stabilising the laser system.
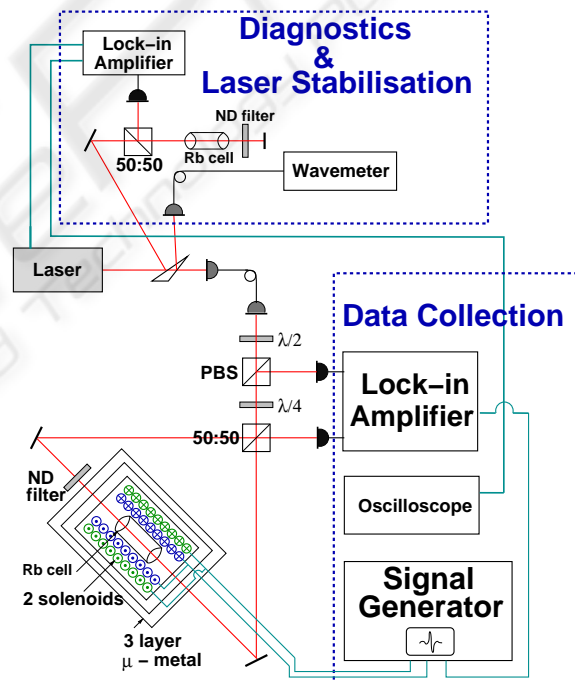


Figure 4: A schematic of the apparatus used in this experiment.

The main design of the experiment is a Sagnac interferometer, which starts a single beam that is then split, these two beams then counterpropagate around a ring. The beams return to their entry point and leave the interferometer where they interact and produce interference fringes.

Before the light enters the interferometer it is coupled into a single mode optical fibre to clean the mode

for the experiment. We use a series of optics to prepare the polarisations before splitting the circular polarised light with a 50:50 beam splitter into the interferometer. It is here we obtain the $\sigma^{+/-}$ terms as displayed in figure 1. Before entering the vapour cell one of the beams is attenuated with a neutral density filter (ND filter), making it into our weak probe beam.

Two solenoids surround the vapour cell within three layers of $\mu$-metal shielding. These are driven by an arbitrary signal generator. The first (modulation) solenoid is driven with a square wave corresponding to approximately 1nT of between 250-300KHz, which is used as the reference for the signal recovery lock-in amplifier. The second solenoid is also connected to the arbitrary signal generator and is driven with a sine wave with frequencies between 2-8Hz. The human heart has a frequency range of 1-1.67Hz, with higher frequency components.

The raw signal is collected via a photodiode and then connected to the input of the signal recovery lock-in amplifier. The lock-in amplifier allows very small signals to be extracted from the large amounts of noise, using this system we have gained sensitivities in the range of a fetal heart beat. An example of test data taken using a simulated heartbeat is displayed in figure 5.
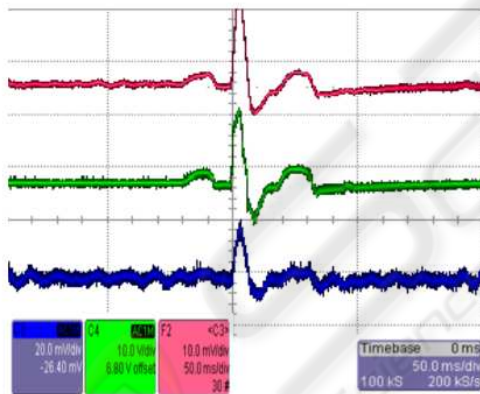


Figure 5: A sceen dump of data take on the experiment. The centre trace is the raw input signal, a simulated QRS, the lower trace is the raw data from the photodiode and the upper trace is the 20 trace avarage.

## 3 CONCLUSIONS

With current data we can measure magnetic fields of the order of a fetal heart beat. The experiment is still at a very early stage of development, therefore the current data acquisition method is not suitable for clinical applications. However even at this stage the experiment has shown a great deal of promise as a potential MCG device. We expect, with some calibration, to obtain at least femtotelsa sensitivities (Fleischhauer and Scully, 1994), with the possibility of using more optical fibres and replacing the modulation solenoid with an alternative scheme such as an acoustic or electro-optic modulator (AOM/EOM). These improvements will move this research closer to being a competitive device for performing clinical MCG trials.

## ACKNOWLEDGEMENTS

## REFERENCES

Belfi, J., Bevilacqua, G., Biancalana, V., Dancheva, Y., and Moi, L. (2007). All optical sensor for automated magnetometry based on coherent population trapping.

Bison, G., Wynands, R., and Weis, A. (2003). Dynamical mapping of the human cardiomagnetic field with a room-temperature, laser-optical sensor. *Opt. Express*, 11(8):904–909.

Bloom, A. L. (1962). Principles of operation of the rubidium vapor magnetometer. *Appl. Opt.*, 1(1):61–68.

Boller, K. J., Imamolu, A., and Harris, S. E. (1991). Observation of electromagnetically induced transparency. *Physical Review Letters*, 66(20):2593+.

Budker, D., Kimball, D. F., Rochester, S. M., Yashchuk, V. V., and Zolotorev, M. (2000). Sensitive magnetometry based on nonlinear magneto-optical rotation. *Physical Review A*, 62(4):043403+.

Cohen-Tannoudji, C., Dupont-Roc, J., Haroche, S., and Laloë, F. (1969). Detection of the static magnetic field produced by the oriented nuclei of optically pumped he3 gas. *Physical Review Letters*, 22(15):758+.

Comani, S., Mantini, D., Alleva, G., Di, L. S., and Romani, G. L. (2004). Fetal magnetocardiographic mapping using independent component analysis. *Institute of Physics Publishing Physiological Measurement*.

Fagaly, R. L. (2006). Superconducting quantum interference device instruments and applications. *Review of Scientific Instruments*, 77(10).

Fenici, R., Romani, G., and Erné, S. (1983). High-resolution magnetic measurements of human cardiac electrophysiological events. *Il Nuovo Cimento D*, 2(2):231–247.

Fleischhauer, M., Imamoglu, A., and Marangos, J. P. (2005). Electromagnetically induced transparency: Optics in coherent media. *Reviews of Modern Physics*, 77(2).

Fleischhauer, M. and Scully, M. O. (1994). Quantum sensitivity limits of an optical magnetometer based on atomic phase coherence. *Physical Review A*, 49(3):1973+.

MAGNETOMETRY USING ELECTROMAGNETICALLY INDUCED TRANSPARENCY IN A ROOM
TEMPERATURE VAPOUR CELL - Developing an Optical Magnetometer that Utilises the Steep Dispersion Curve
Observed in EIT to Detect Time Varying Magnetic Fields

Hämäläinen, M., Hari, R., Ilmoniemi, R. J., Knuutila, J., and Lounasmaa, O. V. (1993). Magnetoencephalography&#151;theory, instrumentation, and applications to noninvasive studies of the working human brain. *Reviews of Modern Physics*, 65(2):413+.

Harris, S. E. (1997). Electromagnetically induced transparency. In *Quantum Electronics and Laser Science Conference, 1997. QELS '97., Summaries of Papers Presented at the*, page 25.

Kominis, I. K., Kornack, T. W., Allred, J. C., and Romalis, M. V. (2003). A subfemtotesla multichannel atomic magnetometer. *Nature*, 422(6932):596–599.

Nagel, A., Graf, L., Naumov, A., Mariotti, E., Biancalana, V., Meschede, D., and Wynands, R. (1998). Experimental realization of coherent dark-state magnetometers. *Europhysics Letters*, pages 31–36.

Nash, M. P., Bradley, C. P., Kardos, A., Pullan, A. J., and Paterson, D. J. (2002). An experimental model to correlate simultaneous body surface and epicardial electropotential recordings in vivo. *Chaos, Solitons & Fractals*, 13(8):1735–1742.

Ramanathan, C., Ghanem, R. N., Jia, P., Ryu, K., and Rudy, Y. (2004). Noninvasive electrocardiographic imaging for cardiac electrophysiology and arrhythmia. *Nat Med*, 10(4):422–428.

Scully, M. O. (1991). Enhancement of the index of refraction via quantum coherence. *Physical Review Letters*, 67(14):1855+.

Vodel, W. and Makiniemi, K. (1992). An ultra low noise dc squid system for biomagnetic research. *Measurement Science and Technology*, 3(12):1155–1160.